

Hydrogen Storage in Palladium Hollow Nanoparticles

Felipe J. Valencia, Rafael I. Gonzalez, Diego Tramontina, Jose Rogan, Juan Alejandro Valdivia, Miguel Kiwi, and Eduardo M Bringa

J. Phys. Chem. C, **Just Accepted Manuscript** • DOI: 10.1021/acs.jpcc.6b07895 • Publication Date (Web): 26 Sep 2016

Downloaded from <http://pubs.acs.org> on September 27, 2016

Just Accepted

“Just Accepted” manuscripts have been peer-reviewed and accepted for publication. They are posted online prior to technical editing, formatting for publication and author proofing. The American Chemical Society provides “Just Accepted” as a free service to the research community to expedite the dissemination of scientific material as soon as possible after acceptance. “Just Accepted” manuscripts appear in full in PDF format accompanied by an HTML abstract. “Just Accepted” manuscripts have been fully peer reviewed, but should not be considered the official version of record. They are accessible to all readers and citable by the Digital Object Identifier (DOI®). “Just Accepted” is an optional service offered to authors. Therefore, the “Just Accepted” Web site may not include all articles that will be published in the journal. After a manuscript is technically edited and formatted, it will be removed from the “Just Accepted” Web site and published as an ASAP article. Note that technical editing may introduce minor changes to the manuscript text and/or graphics which could affect content, and all legal disclaimers and ethical guidelines that apply to the journal pertain. ACS cannot be held responsible for errors or consequences arising from the use of information contained in these “Just Accepted” manuscripts.

Hydrogen Storage in Palladium Hollow Nanoparticles

Felipe J. Valencia,^{†,§} Rafael I. González,^{†,§} Diego Tramontina,[‡] José Rogan,^{†,§}
Juan Alejandro Valdivia,^{†,§} Miguel Kiwi,^{*,†,||} and Eduardo M. Bringa[¶]

[†]*Departamento de Física, Facultad de Ciencias, Universidad de Chile, Casilla 653,
Santiago, Chile 7800024*

[‡]*Facultad de Ciencias Exactas y Naturales, Universidad Nacional de Cuyo,
FCEN-UNCuyo, Mendoza, M5502JMA, Argentina, and Instituto de Bioingeniería,
Universidad de Mendoza, IBio-UM, Mendoza M5502BZG, and Consejo Nacional de
Investigaciones Científicas y Tecnológicas, CONICET, CABA, C1033AAJ, Argentina*

[¶]*Facultad de Ciencias Exactas y Naturales, Universidad Nacional de Cuyo, Mendoza
5500, Argentina, and CONICET, Argentina.*

[§]*Centro para el Desarrollo de la Nanociencia y la Nanotecnología, CEDENNA, Avda.
Ecuador 3493, Santiago, Chile 9170124.*

^{||}*Centro para el Desarrollo de la Nanociencia y la Nanotecnología, CEDENNA, Avda.
Ecuador 3493, Santiago, Chile 9170124. Phone: +562 2978 7290*

E-mail: m.kiwi.t@gmail.com

Abstract

The potential and properties of palladium hollow nanoparticles (hNP) as a possible H storage material are explored by means of classical molecular dynamics (MD) simulations. First we study the stability of pure Pd hNPs for different sizes and thicknesses, obtaining good agreement with experimental results for nanometer size Pd hNP. Next we add, every 100 fs, single H atoms into the NP cavity. During the first stages of the simulation our results show hydride formation on the inner surface, similar to what has been observed in experiments on Pd surfaces and NPs. Formation of the Pd hydride decreases the absorption rate and H gas is formed inside the cavity. The maximum H gas pressure that is reached is of 7 GPa, before fractures appear in the hNP, and consequently the hNP breaks up. We obtain a maximum H/Pd ratio of 1.21 when H is introduced only inside the cavity. However, when H is deposited both on the inside and outside surfaces this ratio reaches 1.70, which is 25% larger than previous reports. Beyond this ratio the hNP breaks up and the H gas is ejected from the hNP cavity.

Introduction

Palladium based structures have attracted much interest for a long time because of their major role in several industrial processes like catalysis, hydrogen storage and gas-sensing. Moreover, during the last years fuel cells based on Pd have been developed,¹ which have potential for many power supply applications in daily use devices, such as vehicles and cellphones. In these areas Pd materials are an economically and competitive choice, especially when compared with other noble metals such as Pt.

In particular, the development of Pd nanostructures with large H storage capacity has been investigated for a variety of configurations such as nanowires,² nanorods, nanocubes³ and nanoparticles,⁴⁻⁶ offering better performance than bulk structures,⁷ thin films⁸ and grain boundaries.⁹ Among all these morphologies NP show promising advantages for H storage, due their large surface to volume ratio, which allows for increased H capture. This led to

1
2
3 many theoretical and experimental studies on the NP palladium H storage mechanism, and
4 their variations with shape and size.^{5,10-13}
5
6

7 Lately hNP, which have a significantly lower density and a large specific area in compari-
8 son to conventional NPs, have attracted special attention due their potential applications in
9 fields like catalysis, storage, sensors,¹⁴ drug delivery,^{15,16} and energy related devices. More-
10 over, recent experimental work has confirmed the potential of hNP as storage material. In
11 fact, hNP of different materials such as Fe₂O₃,^{17,18} SnO₂,¹⁹ Si,²⁰ and TiO₂²¹ have shown
12 promissory results for Lstorage,^{17,18} which are essential for the development of efficient
13 lithium batteries. Additionally, the H storage of Li₂NH hNP has been explored and shows
14 an enhanced kinetics,²² probably due to features like short diffusion distance and/or large
15 surface area. These nanostructures can absorb a large amount of H in a shorter time than
16 micrometer size particles. Moreover, the hydrogen desorption temperature can decrease by
17 ≈100 K when compared to the bulk. Other examples are carbon and mesoporous carbon
18 hNP decorated with Pd NPs,^{23,24} which exhibit a larger storage capacity than pristine sam-
19 ples, reaching an increase of a factor of two of H weight. This has led us to investigate the
20 feasibility of the use Pd hNP as a H storage material because of its H dissociation capacity
21 under ambient conditions.
22
23
24
25
26
27
28
29
30
31
32
33
34
35
36
37

38 Currently, these Pd hNP are synthesized by many groups, in a wide range of sizes.^{14,25} For
39 example, Liu *et al.*²⁶ reported raspberry-like hNP of 32 nm in diameter implanted in carbon
40 nanotubes. Other groups reported hNP with porous shells ≈25 nm in diameter created
41 by the galvanic replacement method,²⁷ or of ≈19 nm by the coalescence of smaller NPs.²⁸
42 Moreover, in the last years smaller quasi-spherical hNP have been fabricated by the reduction
43 technique,²⁹ with an average diameter of 7.3 nm, but their thickness was not reported. All
44 these sizes are within the scope of classical molecular dynamics (MD) simulations, which can
45 provide an accurate description of their mechanical and thermal properties.
46
47
48
49
50
51
52
53

54 Our main objective is the study of the H storage capacity of these hNPs. To achieve
55 our goal we deposit, one by one, H atoms in the hNP cavity until saturation is reached. To
56
57
58
59
60

1
2
3 start on a firm basis we obtain, by means of MD simulations, the thermal and mechanical
4 properties of hNP at 300 K. Since defects are generated during the hydrogenation process
5 we also investigate how they form.
6
7
8
9

10 11 12 13 14 15 16 17 18 19 20 21 22 23 24 25 26 27 28 29 30 31 32 33 34 35 36 37 38 39 40 41 42 43 44 45 46 47 48 49 50 51 52 53 54 55 56 57 58 59 60

In order to understand the thermal and structural properties of Pd hNPs we use classical MD simulations, as implemented in the LAMMPS code.³⁰ The simulations were carried out using the embedded atom³¹ (EAM) potential, with the Zhou³² parametrization. The hNP was created by cutting a spherical cavity from a fcc Pd $\langle 100 \rangle$ bulk. This quasi-spherical geometry is characterized by the external radius R_{ext} and the shell thickness w . The range of radii studied is $6a_0 \leq R \leq 60a_0$ ($2.4 \leq R \leq 24$ nm), and thicknesses between $a_0 \leq w \leq 6a_0$ ($0.4 \leq w \leq 2.4$ nm), where $a_0 = 3.89$ Å is the Pd lattice parameter. Initially, alternating the Fast Inertial Relaxation Engine³³ (FIRE) and the Conjugate Gradient algorithms, in order to achieve the best possible putative minimum energy conformation. To study the thermal stability of these nanostructures the temperature of the system was varied from 0 to 300 K, with an increase of 20 K every 0.2 ns. The system temperature was controlled by a Nose-Hoover thermostat, and a time-step of 1 fs was adopted.

To estimate the H storage capacity of these structures atomic H was inserted into the hNP hole. In some experimental situations, H would be incorporated to the hNP from the outside. This would be extremely costly computationally. As an alternative, we have chosen to model the incorporation of H from the inside of the hNP, which allows faster H incorporation. Therefore, to estimate the H storage capacity of these structures atomic H was inserted directly into the hNP hole. However, the EAM potential does not provide realistic results because the H-H interaction allows for the formation of H nanoclusters in the gas phase. A more realistic treatment for H in the gas phase is given by the ReaxFF potential³⁴ with the Senftle parametrization.³⁵ This potential has been fitted to reproduce

hydrogen dissociation and migration in Pd, and has shown to be in good agreement with experiments^{36,37} of H absorption from the gas phase, and the Pd NPs diffusion coefficients. The reactive nature of ReaxFF allows to reproduce correctly the H-H interaction, without yielding the formation of H agglomerates. H was deposited at random at a distance of $0.5 a_0$ from the inner hNP surface. Due to the mass difference between H and Pd an adaptive time-step between 0.1 and 0.25 fs was chosen. The H pressure is computed evaluating the stress tensor, given by the relation

$$p_i^{\alpha\beta} = -\frac{1}{3}\text{Tr} \left[\frac{m_i v_i^\alpha v_j^\beta + \sum_{i \neq j} F_{ij}^\alpha r_{ij}^\beta}{\Omega_i} \right], \quad (1)$$

where the first term is the thermal contribution, v_i^α is the α component of the i -th atom velocity, Ω_i is the atomic volume, and F_{ij} and r_{ij} are the force and distance between atom i and j , respectively. The atomic volume Ω_i is estimated on the basis of the Pauling radius³⁸ assuming spherical atomic shape. This assumption yields similar results to other algorithms used to evaluate the atomic volume, as Voronoi tessellation.³⁹ Defects and/or fractures resulting from the H absorption, and the consequent pressure increase it generates, has been studied using the common neighbor analysis (CNA) algorithm,⁴⁰ which is the one implemented in the Open Visualization Tool⁴¹ (OVITO). In addition, a more refined description of the crystal structure was obtained with the Crystal Analysis Tool⁴² (CAT), which is a set of algorithms that advantageously use several post-processing defect recognition methods, to generate a unique signature for each microstructure. These signatures are then matched against a pattern database which not only contains information, but also allows to determine the atomic positions relative to other crystalline structures, by means of graph maps.

Results

Since our first objective is to describe the thermal stability of hNP we start with perfect spherical hNPs of different sizes and thicknesses. As suggested by Jiang *et al.*,⁴³ when the

1
2
3
4 hNP temperature is raised from 0 to 300 K the initial configuration can reach three possible
5
6 final outcomes: i) a stable hNP, when it keeps its shape at the end of the temperature ramp;
7
8 ii) an unstable configuration, if it collapses to form a deformed solid NP at temperatures
9
10 above 300 K; and finally iii) a half-stable hNP, which is defined as a partial collapse of the
11
12 initial configuration that maintains a cavity in its interior. The results for the different ratios
13
14 and thicknesses w we studied are illustrated in Fig. 1, where we provide a stability diagram
15
16 for different sizes and thicknesses that are in agreement with experimental results.^{28,29} The
17
18 figure shows an unstable region for $w \leq 3a_0$ (red circles); a stable region (green circles);
19
20 half-stable hNPs (blue circles) are found only for large values of the aspect ratio, which is
21
22 defined as R_{ext}/w . We also show an A zone where our theoretical values are consistent with
23
24 the experimental results by Wang *et al.* for 25 nm NPs. For small hNPs the experiments
25
26 by Chen *et al.*²⁹ reported 7 nm diameter hNPs, however they did not provide the values of
27
28 w . Our MD simulations yield that these hNPs have a minimal $w \approx 1.5$ nm. The D regions
29
30 correspond to the experimental results by Ge *et al.*,²⁸ who used the same synthesis protocol
31
32 to obtain two different sized Pd hNP of ≈ 40 nm and ≈ 15 nm in diameter, by changing the
33
34 ph of the concentration. For 40 nm diameter they report a thickness of 8 nm. Instead, in
35
36 our calculations we obtain 40 nm hNP with a minimal thickness of ≈ 2.1 nm. This suggests
37
38 that it might be possible to synthesize thinner hNPs.
39

40 All in all the structures mentioned above, and illustrated in Fig. 1, were followed during
41
42 long computer runs to ensure that they preserve their atomic structure, and are stable over
43
44 large time periods. These calculations followed the scheme developed by Jiang *et al.*⁴³ but
45
46 with a significantly more extended in time temperature ramp. In all cases we made sure that
47
48 the atomic structure, potential energy and the mean square displacement remained constant.
49
50
51
52
53
54
55
56
57
58
59
60

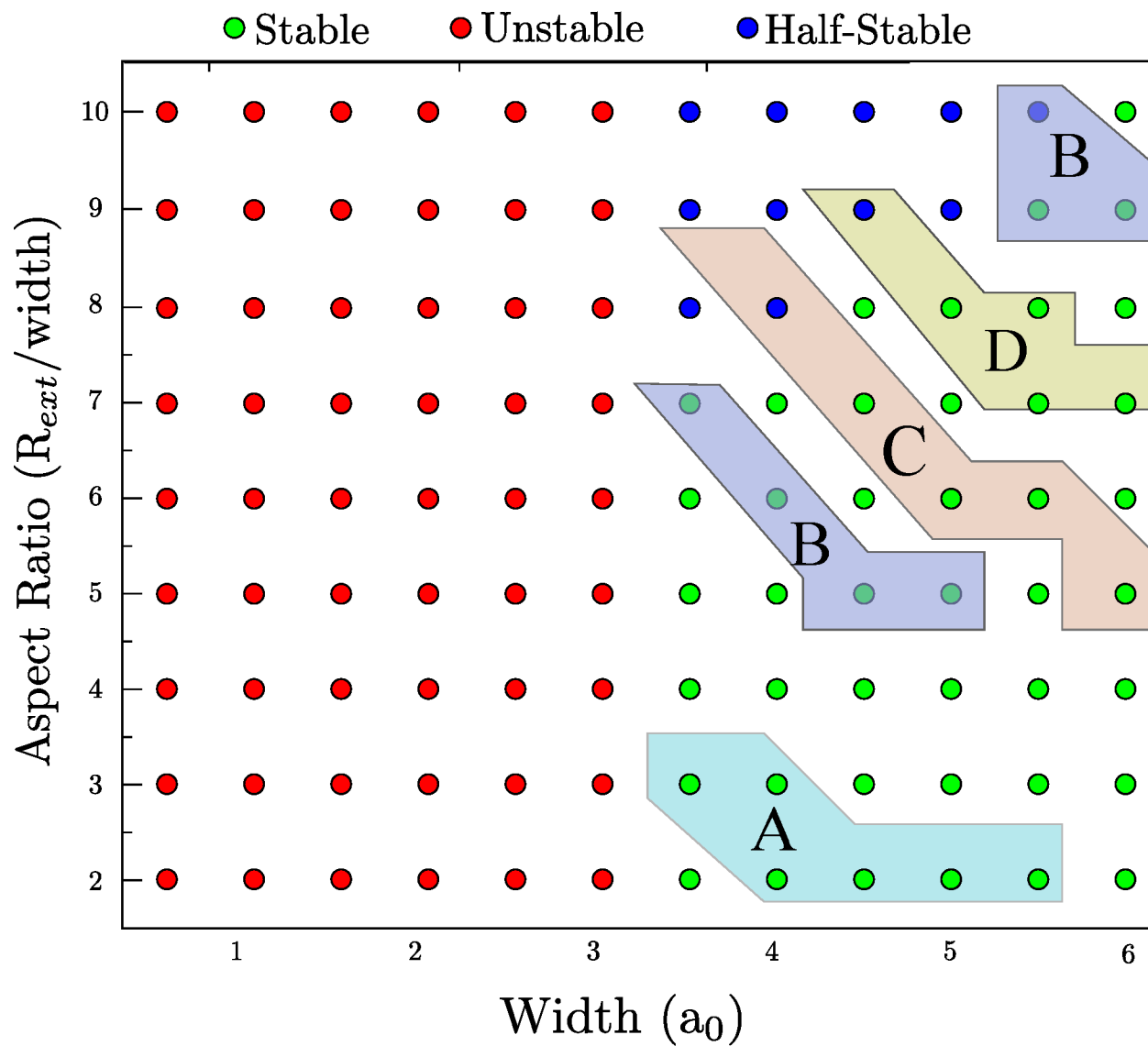
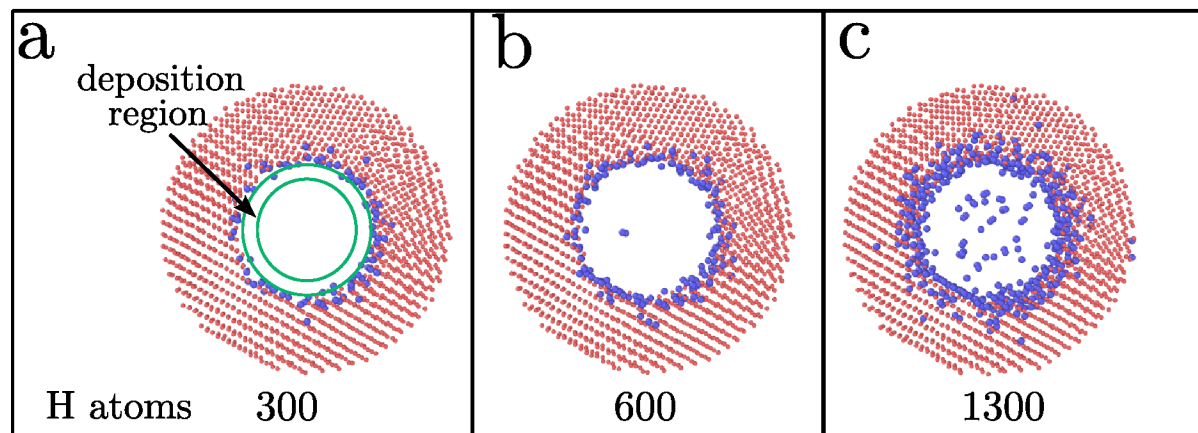


Figure 1: Stability diagram for Palladium nanoclusters using the EAM potential. The B region is in agreement with experimental results by Chen *et al.*²⁹ A corresponds to the experimental results reported by Wang *et al.*,²⁷ and C and D correspond to the results of Liu *et al.*²⁶ and Ge *et al.*,²⁸ respectively.

To study the H absorption we chose a 7528 Pd atom hNP with inner and outer radii $R_{in} = 4a_0$ and $R_{out} = 8a_0$, respectively. This hNP is well within the stability range of the diagram of Fig. 1, so as to exclude a possible collapse due to the embrittlement caused by the H absorption. Since the H-H interaction at high densities is not realistically described by EAM, a reactive potential such as ReaxFF is a more adequate tool to model the system. However, the significant computational time required by ReaxFF makes it costly to model

1
2
3
4 large hNPs. Because of this reason the stability results for Pd hNPs were obtained with the
5
6 Zhou potential,³² that has been used as a reference for ReaxFF calculations. After raising
7
8 the temperature of the initial structure from 0 to 300 K, during 0.2 ns, the results yield
9
10 stable hNPs, both for ReaxFF and EAM, for a hNP of $R_{\text{in}} = 4a_0$ and $R_{\text{out}} = 8a_0$.

11
12 Fig. 2 illustrates the initial H deposition stages into the hNP cavity, showing that the
13
14 saturation of subsurface octahedral and tetrahedral sites takes place first, followed by the
15
16 saturation of the inner surface region. When the H atom absorption increases a Pd hydride
17
18 is seen to form on the inner surface, this way reducing the inner cavity radius by almost
19
20 2 \AA due to the Pd NP expansion; however, the hNP does not collapse. As a consequence
21
22 of the formation of Pd hydride the H absorption rate diminishes, and some of the atoms
23
24 deposited are repelled from the inner shell towards the hNP cavity center, as seen in Fig. 2b.
25
26 The fact that the absorption time is reduced relative to the deposition time, due to hydride
27
28 formation, promotes the formation of H_2 molecules, which creates a H gas phase in the cavity,
29
30 as shown in Fig 2c.



47
48
49
50
51
52
53
54
55
56
57
58
59
60

Figure 2: Cross section of Pd hNP (red atoms) used for the MD simulation of H (blue atoms) deposition. After 600 single atom depositions the H atoms are repelled from the inner surface towards the center of the cavity. After 1300 H atoms are deposited H_2 molecules and H atoms are observed in center of cavity.

In Fig. 3a we compare the H deposition with the H gas storage rates inside the cavity, as a function of time. For small values of the H/Pd ratio all the H is absorbed in Pd interstitial sites; when $\text{H}/\text{Pd} \approx 0.2$ an abrupt increase of H in the NP cavity is observed, which coincides

1
2
3 with the formation of the Pd hydride. For large values of H/Pd both the total and the cavity
4 H have similar growth rates, thus the number of H₂ molecules and the H gas pressure do
5 increase. The hydride helps to avoid the dissociation of H₂ molecules catalyzed by the Pd
6 atoms. For H/Pd > 0.2 the mechanism for H insertion changes due to kinetic effects, as a
7 consequence of the collisions of high speed H₂ molecules with H atoms. The collision of H₂
8 molecules with H atoms accelerates the latter enough to cross the inner hydride surface and
9 to reach the outer layer of the hNP. Such a process was already reported for large values of
10 the chemical potential, obtained by Monte Carlo simulations.^{8,11-13}

11
12 The increment of the H density in the cavity results in a increase of the H pressure, which
13 is not negligible for H/Pd > 0.2. The response of the structure to the pressure increase is
14 a slow expansion of the hNP, whose radius grows by $\approx 2 \text{ \AA}$. In Fig. 3b we show that the
15 maximum internal pressure that a hNP can withstand is 7 GPa; for larger H/Pd ratios the
16 pressure in the cavity decreases drastically to $\approx 3 \text{ GPa}$. This abrupt decrease is a consequence
17 of structural changes in the hNP, such as creation of defects, amorphous regions and stacking
18 faults, which will be discussed below.

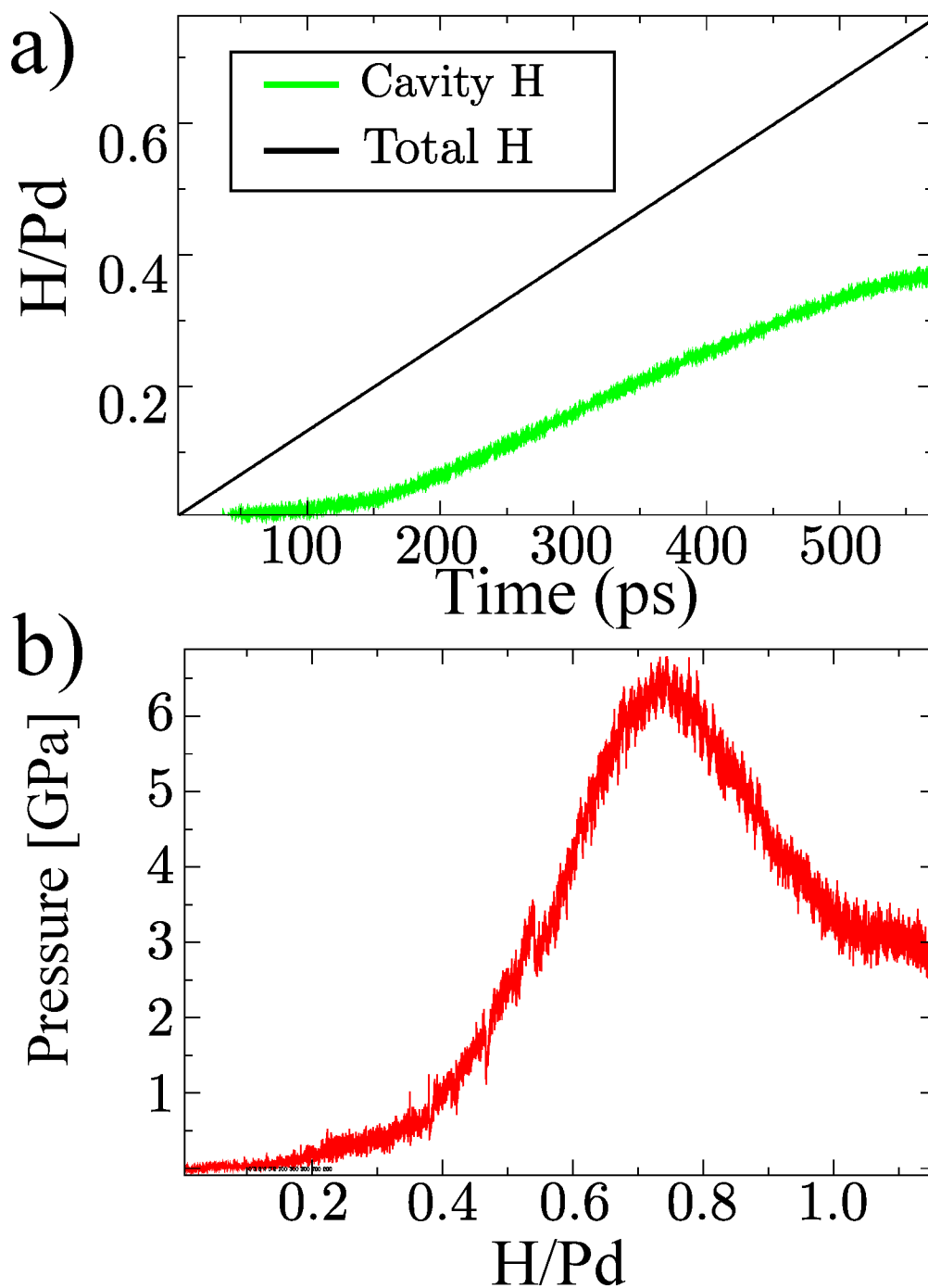
19
20 The response to pressure of the hNP as a function of the H/Pd ratio is illustrated in
21 Fig 4. A common neighbor analysis (CNA) was performed before and after the pressure
22 reached the 7 GPa peak. The pressure inside the cavity starts to create point defects in
23 the Pd structure for H/Pd < 0.75, as shown in Fig 4a. These defects correspond to isolated
24 bcc atoms near to the inner hNP radius; the red color atoms correspond to non-crystalline
25 structures that are not well defined, since for surface atoms they are not recognized as such
26 by the CNA algorithm, as they lack the necessary coordination to be identified as fcc. On the
27 inner radius the red region is wider than the surface one, due the formation of Pd hydride.
28 For H/Pd=0.75 the hNP has also lost its spherical form, as shown in Fig. 4c. A non uniform
29 width results, with a thinner region that has no definite crystalline structure. This region
30 corresponds mainly to Pd hydride with some free volume regions, as shown in Fig. 4d. It is
31 worth noticing that the porosity allows for a larger H storage capacity of the hNP. Moreover,
32
33
34
35
36
37
38
39
40
41
42
43
44
45
46
47
48
49
50
51
52
53
54
55
56
57
58
59
60

1
2
3
4 for these concentrations we observe a different scenario, where groups of hcp regions are seen
5
6 in the Pd lattice. This hcp phase, whose occurrence in fcc crystals is principally associated
7
8 with stacking faults, has been reported by Huang *et al.*⁴⁴ in AgPt hNPs, and is associated
9
10 to Shockley partial dislocations, due to the large stress the hollow-core-shell structure is
11
12 subjected to. In our case, the large stress produced by the H pressure can generate a series
13
14 of planar defects, which under normal conditions are difficult to induce due the large energy
15
16 required by Pd to generate stacking faults. This large population of hcp atoms are observed
17
18 in the transition from stable to half-stable hNP in Pd (see supplementary material), and
19
20 they are probably responsible for avoiding the collapse of the hNP into a simple NP. Fig. 4e
21
22 shows a CAT analysis where pattern-matching was performed including defective structures
23
24 from a large database.⁴² The fraction of fcc atoms obtained this way corresponds to 66.76%,
25
26 and to 5.42% of fcc stacking faults and twins boundaries.

27
28 The feasibility to decorate the cavity of a Pd hNP has been tested by a single deposition
29
30 process, resulting in a maximum H/Pd=1.21. Beyond this limit the hNP breaks up, and the
31
32 H inside cavity is ejected. However the hNP does not collapse, and a partial surface recovery
33
34 is observed. The simulation was carried out during 0.2 ns, in order to be able follow the
35
36 structural evolution of the hNP and the recovery of the surface. The fact that the hNP does
37
38 not collapse after the H is released is a promising feature when one considers the possibility
39
40 of reusing this kind of nanostructures. On the other hand, if the hNP cavity is preserved
41
42 after the H ejection, both the inner and outer surface would be able to capture H, enhancing
43
44 the hNP H storage capacity under ambient conditions.

45
46 Finally, to estimate the maximum H/Pd storage performance of Pd hNP we changed
47
48 slightly the procedure. We started with a hNP with a H/Pd ratio of 1.1, which insures
49
50 no material failure. This hNP was immersed in a H atmosphere, in order to accelerate the
51
52 calculations. The H atoms occupy the free sites on the outer surface of the hNP allowing the
53
54 H/Pd ratio to rise to 1.70, as illustrated in Fig. 5. To insure stability the dynamics was fol-
55
56 lowed during ≈ 0.2 ns. To the best of our knowledge this is the largest value reported for a Pd
57
58
59
60

1
2
3 nanostructure, since the previous one, obtained by means of Monte Carlo simulations,^{8,11-13}
4
5 is 1.33.
6
7



53 Figure 3: a) Deposition rate as function of time. The green curve corresponds to the H
54 storage inside the cavity of the hNP. b) Pressure in the cavity as a function of the H/Pd
55 ratio.
56
57
58
59
60

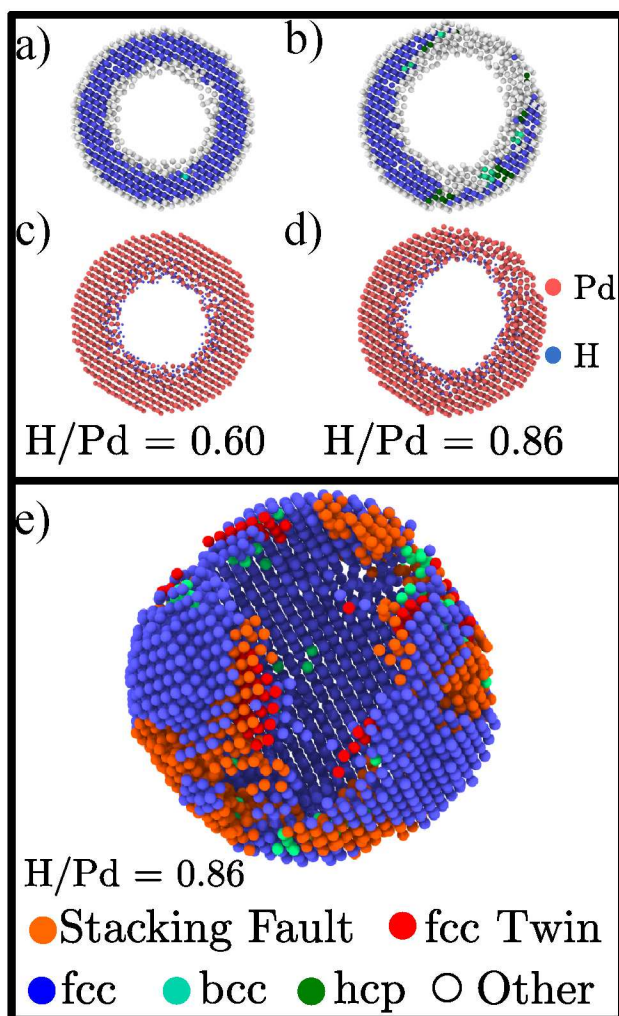


Figure 4: a), b), c) and d) show a cross section of the hNP. a) and b) show a Common Neighbor Analysis (CNA) for two different Pd/H ratios. In c) and d) we observe the H distribution inside the Pd lattice. e) Show a CAT analysis of the hNP with a H/Pd=0.89, atoms with a structure type different of fcc or bcc were deleted of the picture.

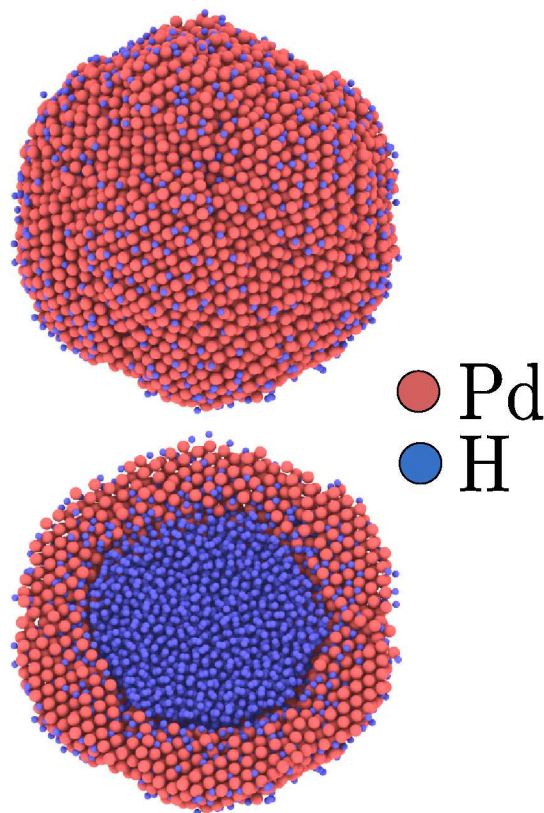


Figure 5: hNP after the H/Pd=1.7 concentration is reached. Blue and red correspond to H and Pd, respectively. The top pannel corresponds to the outer surface, and the lower one to an equatorial cut.

Discussion and Conclusions

By means of molecular dynamics simulations we investigate the stability of Pd hNP, from 0.3 to 2.3 nm in thickness and less than 42 nm in diameter. Our stability diagram shows that it is possible to observe a transition of the hNP from unstable to stable when a thickness $w \approx 1.17$ nm is reached (which corresponds to $3a_0$ in Fig. 1). For $w > 1.17$ nm the hNP stability increases. For $w < 1.17$ nm the hNP tends to collapse, and form a solid NP. This result is similar to the one reported by Jiang *et al.*⁴⁵ for Au hNP. In fact, our simulations predict stable hNP with diameters larger than 5.5 nm and a minimum thickness of 1.4 nm, smaller than those reported by Chen *et al.*²⁹ The largest hNP we studied are 42 nm in diameter and $w > 2.3$ nm establishing a lower limit for the Pd hNP synthesized by Ge *et*

1
2
3 *al.*²⁸ of 40 nm with a thickness of 8 nm. Other experimental results, as those reported by
4
5 Liu *et al.*²⁶ and Wang *et al.*²⁷ also correspond to stable Pd hNP in our diagram.
6

7
8 On the other hand, the H storage properties of hNP have been tested, introducing single
9
10 H atoms into the hNP cavity. Our results show that the cavity can store H in the form of
11
12 single atoms or as a H gas phase. This gas phase is achieved when Pd hydride is formed
13
14 on the inner surface and the deposition rate is larger than the H absorption rate. The
15
16 hNP studied here can withstand a H pressure of up to 7 GPa. Beyond this limit the hNP
17
18 changes its shape in order to relax the large stress the H₂ gas pressure generates. The defects
19
20 observed correspond mainly to stacking faults and twins. The latter ones have been reported
21
22 to induce ultrahigh hardening of Pd thin films.⁴⁶ This way the maximum H/Pd ratio of 1.21
23
24 is reached. Beyond this limit the hNP breaks up, and H₂ its ejected from the cavity. As the
25
26 H is released the hNP partially recovers without collapsing.
27

28
29 Finally, a maximum H/Pd=1.7 ratio is obtained when single H atoms are deposited on
30
31 the outer and inner surfaces of the hNP. This ratio is the largest yet reported and is 25%
32
33 larger than the results for an icosahedron cluster obtained by Crespo *et al.*¹¹ However, we
34
35 believe that this results could be improved, for example using MC simulations to decorate
36
37 the Pd interstitial sites.^{8,11-13}

38
39 Summarizing, we studied the efficiency of Pd hNPs to store H inside their cavities and in
40
41 the whole structure. However, important questions that do deserve attention remain open,
42
43 such as the details of the diffusion mechanism in this kind of nanostructures. It also may
44
45 be that the presence of stacking faults and/or twins helps to increase the H migration and
46
47 absorption. But, for the time being, our results suggest that the use of the cavity of a hNP
48
49 as a gas storage material is a possibility, and a subject that deserves attention.
50
51
52
53
54
55
56
57
58
59
60

Acknowledgments

This work was supported by the Fondo Nacional de Investigaciones Científicas y Tecnológicas (FONDECYT, Chile) under grants #3140526 (RG), #1160639 and 1130272 (MK and JR), and Financiamiento Basal para Centros Científicos y Tecnológicos de Excelencia FB-0807 (RG, FV, JM, MK and JR). EMB and DT thank support from PICT-2014-0696 (ANPCyT) and M003 (SeCTyP-UN Cuyo) grant. DT was supported by CONICET Postdoctoral Fellowship Grant and ANPCyT PICT-2015-0040. FV was supported by CONICYT Doctoral Fellowship grant #21140948.

References

- (1) Antolini, E. Palladium in Fuel Cell Catalysis. *Energy & Environmental Sci.* **2009**, *2*, 915–931.
- (2) He, J.; Knies, D.; Hubler, G.; Grabowski, K.; Tonucci, R.; Dechiaro, L. Hydrogen Segregation and Lattice Reorientation in Palladium Hydride Nanowires. *Appl. Phys. Lett.* **2012**, *101*, 153103.
- (3) Nie, G.; Lu, X.; Lei, J.; Yang, L.; Bian, X.; Tong, Y.; Wang, C. Sacrificial Template-Assisted Fabrication of Palladium Hollow Nanocubes and Their Application in Electrochemical Detection toward Hydrogen Peroxide. *Electrochimica Acta* **2013**, *99*, 145–151.
- (4) Narehood, D.; Kishore, S.; Goto, H.; Adair, J.; Nelson, J.; Gutierrez, H.; Eklund, P. X-ray Diffraction and H-storage in Ultra-Small Palladium Particles. *Int. J. Hydrogen Energy* **2009**, *34*, 952–960.
- (5) Wolf, R. J.; Lee, M. W.; Ray, J. R. Pressure-Composition Isotherms for Nanocrystalline Palladium Hydride. *Phys. Rev. Lett.* **1994**, *73*, 557.

- 1
2
3
4
5
6
7
8
9
10
11
12
13
14
15
16
17
18
19
20
21
22
23
24
25
26
27
28
29
30
31
32
33
34
35
36
37
38
39
40
41
42
43
44
45
46
47
48
49
50
51
52
53
54
55
56
57
58
59
60
- (6) Yamauchi, M.; Ikeda, R.; Kitagawa, H.; Takata, M. Nanosize Effects on Hydrogen Storage in Palladium. *J. of Physical Chemistry C* **2008**, *112*, 3294–3299.
- (7) Conrad, H.; Ertl, G.; Latta, E. Adsorption of Hydrogen on Palladium Single Crystal Surfaces. *Surface Sci.* **1974**, *41*, 435–446.
- (8) Ramos De Debiaggi, S.; Crespo, E.; Braschi, F.; Bringa, E.; Al, M.; Ruda, M. Hydrogen Absorption in Pd Thin-Films. *Int. J. Hydrogen Energy* **2014**, *39*, 8590–8595, cited By 0.
- (9) Kuji, T.; Matsumura, Y.; Uchida, H.; Aizawa, T. Hydrogen Absorption of Nanocrystalline Palladium. *J. of Alloys and Compounds* **2002**, *330*, 718–722.
- (10) Pundt, A.; Dornheim, M.; Guerdane, M.; Teichler, H.; Ehrenberg, H.; Reetz, M.; Jisrawi, N. Evidence for a Cubic-to-Icosahedral Transition of Quasi-Free Pd-H-Clusters Controlled by the Hydrogen Content. *The European Physical Journal D-Atomic, Molecular, Optical and Plasma Physics* **2002**, *19*, 333–337.
- (11) Crespo, E. A.; Ruda, M.; de Debiaggi, S. R.; Bringa, E. M.; Braschi, F. U.; Bertolino, G. Hydrogen Absorption in Pd Nanoparticles of Different Shapes. *Int. J. Hydrogen Energy* **2012**, *37*, 14831–14837.
- (12) Crespo, E.; Claramonte, S.; Ruda, M.; de Debiaggi, S. R. Thermodynamics of Hydrogen in Pd Nanoparticles. *Int. J. Hydrogen Energy* **2010**, *35*, 6037–6041.
- (13) Ruda, M.; Crespo, E.; de Debiaggi, S. R. Atomistic Modeling of H Absorption in Pd Nanoparticles. *J. of Alloys and Compounds* **2010**, *495*, 471–475.
- (14) Liang, H.-P.; Lawrence, N. S.; Wan, L.-J.; Jiang, L.; Song, W.-G.; Jones, T. G. Controllable Synthesis of Hollow Hierarchical Palladium Nanostructures with Enhanced Activity for Proton/Hydrogen Sensing. *J. of Phys. Chem. C* **2008**, *112*, 338–344.

- 1
2
3
4 (15) Son, S. J.; Bai, X.; Lee, S. B. Inorganic Hollow Nanoparticles and Nanotubes in
5 Nanomedicine: Part 1. Drug/gene Delivery Applications. *Drug Discovery Today* **2007**,
6 *12*, 650–656.
7
8
9
10 (16) Son, S. J.; Bai, X.; Lee, S. B. Inorganic Hollow Nanoparticles and Nanotubes in
11 Nanomedicine: Part 2: Imaging, Diagnostic, and Therapeutic Applications. *Drug Dis-*
12 *covery Today* **2007**, *12*, 657–663.
13
14
15
16
17 (17) Koo, B.; Xiong, H.; Slater, M. D.; Prakapenka, V. B.; Balasubramanian, M.; Podsi-
18 adlo, P.; Johnson, C. S.; Rajh, T.; Shevchenko, E. V. Hollow Iron Oxide Nanoparticles
19 for Application in Lithium Ion Batteries. *Nano Lett.* **2012**, *12*, 2429–2435.
20
21
22
23
24 (18) Wang, B.; Chen, J. S.; Wu, H. B.; Wang, Z.; Lou, X. W. Quasiemulsion-Templated
25 Formation of α -Fe₂O₃ Hollow Spheres with Enhanced Lithium Storage Properties. *J.*
26 *American Chem. Soc.* **2011**, *133*, 17146–17148.
27
28
29
30
31 (19) Lou, X. W.; Wang, Y.; Yuan, C.; Lee, J. Y.; Archer, L. A. Template-free Synthesis
32 of SnO₂ Hollow Nanostructures with High Lithium Storage Capacity. *Adv. Materials*
33 **2006**, *18*, 2325–2329.
34
35
36
37
38 (20) Ma, H.; Cheng, F.; Chen, J.-Y.; Zhao, J.-Z.; Li, C.-S.; Tao, Z.-L.; Liang, J. Nest-
39 like Silicon Nanospheres for High-Capacity Lithium Storage. *Adv. Materials* **2007**, *19*,
40 4067–4070.
41
42
43
44
45 (21) Chen, J. S.; Luan, D.; Li, C. M.; Boey, F. Y. C.; Qiao, S.; Lou, X. W. TiO₂ and SnO
46 2@ TiO₂ Hollow Spheres Assembled from Anatase TiO₂ Nanosheets with Enhanced
47 Lithium Storage Properties. *Chem. Comm.* **2010**, *46*, 8252–8254.
48
49
50
51
52 (22) Xie, L.; Zheng, J.; Liu, Y.; Li, Y.; Li, X. Synthesis of Li₂NH Hollow Nanospheres with
53 Superior Hydrogen Storage Kinetics by Plasma Metal Reaction. *Chem. of Materials*
54 **2007**, *20*, 282–286.
55
56
57
58
59
60

- 1
2
3
4 (23) Zielinska, B.; Michalkiewicz, B.; Mijowska, E.; Kalenczuk, R. J. Advances in Pd
5 Nanoparticle Size Decoration of Mesoporous Carbon Spheres for Energy Application.
6 *Nanoscale Res. Lett.* **2015**, *10*, 430.
7
8
9
10 (24) Wenelska, K.; Michalkiewicz, B.; Gong, J.; Tang, T.; Kaleńczuk, R.; Chen, X.; Mi-
11 jowska, E. In situ Deposition of Pd Nanoparticles with Controllable Diameters in Hollow
12 Carbon Spheres for Hydrogen Storage. *Int. J. Hydrogen Energy* **2013**, *38*, 16179–16184.
13
14
15
16
17 (25) Kim, S.-W.; Kim, M.; Lee, W. Y.; Hyeon, T. Fabrication of Hollow Palladium Spheres
18 and their Successful Application to the Recyclable Heterogeneous Catalyst for Suzuki
19 Coupling Reactions. *J. American Chem. Soc.* **2002**, *124*, 7642–7643.
20
21
22
23
24 (26) Liu, Z.; Zhao, B.; Guo, C.; Sun, Y.; Shi, Y.; Yang, H.; Li, Z. Carbon Nan-
25 otube/Raspberry Hollow Pd Nanosphere Hybrids for Methanol, Ethanol, and Formic
26 Acid Electro-Oxidation in Alkaline Media. *J. Colloid and Interface Sci.* **2010**, *351*,
27 233–238.
28
29
30
31
32
33 (27) Wang, B.; Yang, J.; Wang, L.; Wang, R.; Tian, C.; Jiang, B.; Tian, M.; Fu, H. Hollow
34 Palladium Nanospheres with Porous Shells Supported on Graphene as Enhanced Elec-
35 trocatalysts for Formic Acid Oxidation. *Phys. Chem. Chem. Phys.* **2013**, *15*, 19353–
36 19359.
37
38
39
40
41
42 (28) Ge, J.; Xing, W.; Xue, X.; Liu, C.; Lu, T.; Liao, J. Controllable Synthesis of Pd
43 Nanocatalysts for Direct Formic Acid Fuel Cell (DFAFC) Application: from Pd Hollow
44 Nanospheres to Pd Nanoparticles. *J. of Phys. Chem. C* **2007**, *111*, 17305–17310.
45
46
47
48
49 (29) Chen, D.; Cui, P.; He, H.; Liu, H.; Yang, J. Highly Catalytic Hollow Palladium Nanopar-
50 ticles Derived from Silver@SilverPalladium CoreShell Nanostructures for the Oxidation
51 of Formic Acid. *J. of Power Sources* **2014**, *272*, 152 – 159.
52
53
54
55
56 (30) Plimpton, S. Fast Parallel Algorithms for Short-Range Molecular Dynamics. *J. of*
57 *Comp. Phys.* **1995**, *117*, 1 – 19.
58
59
60

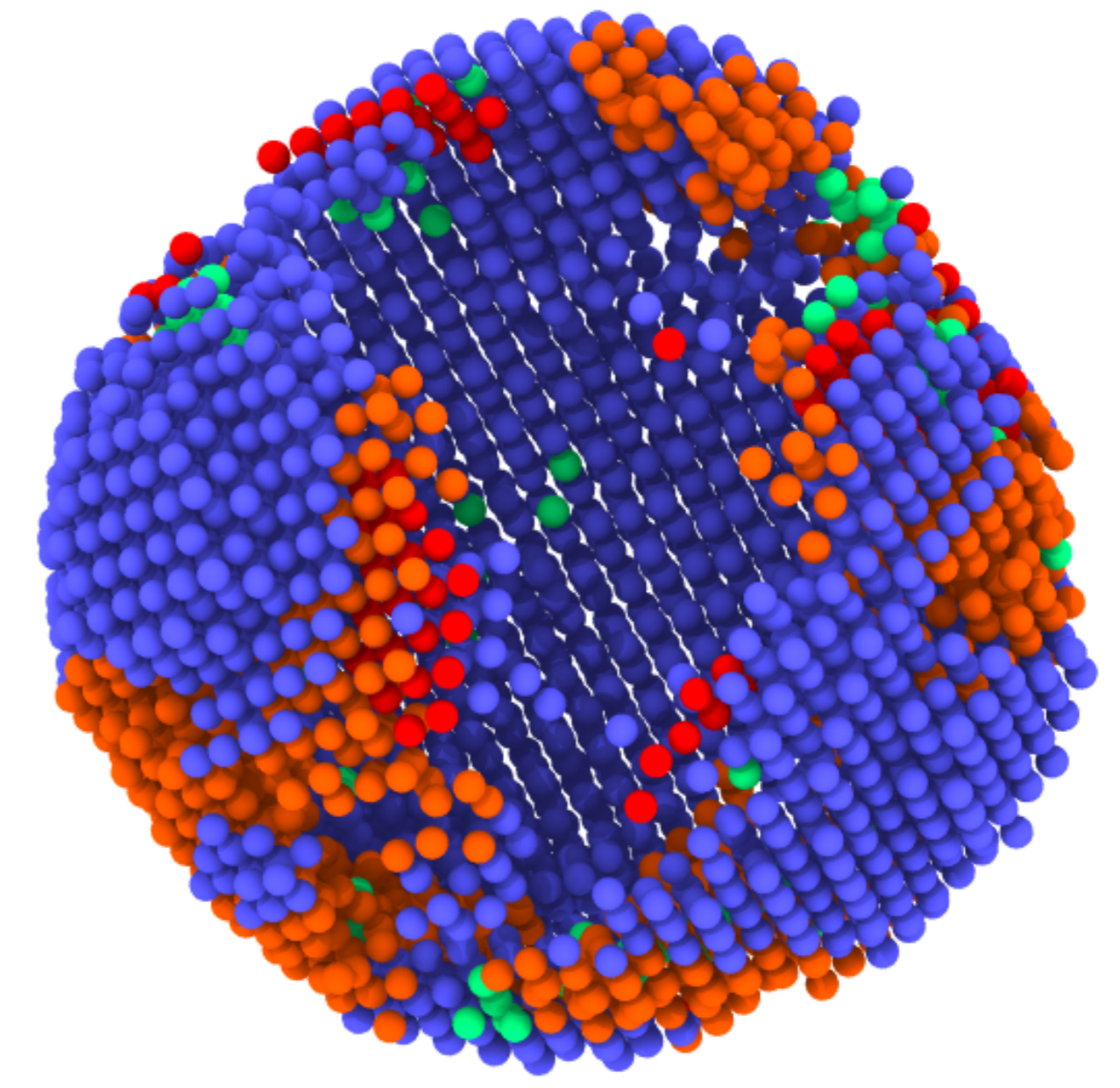
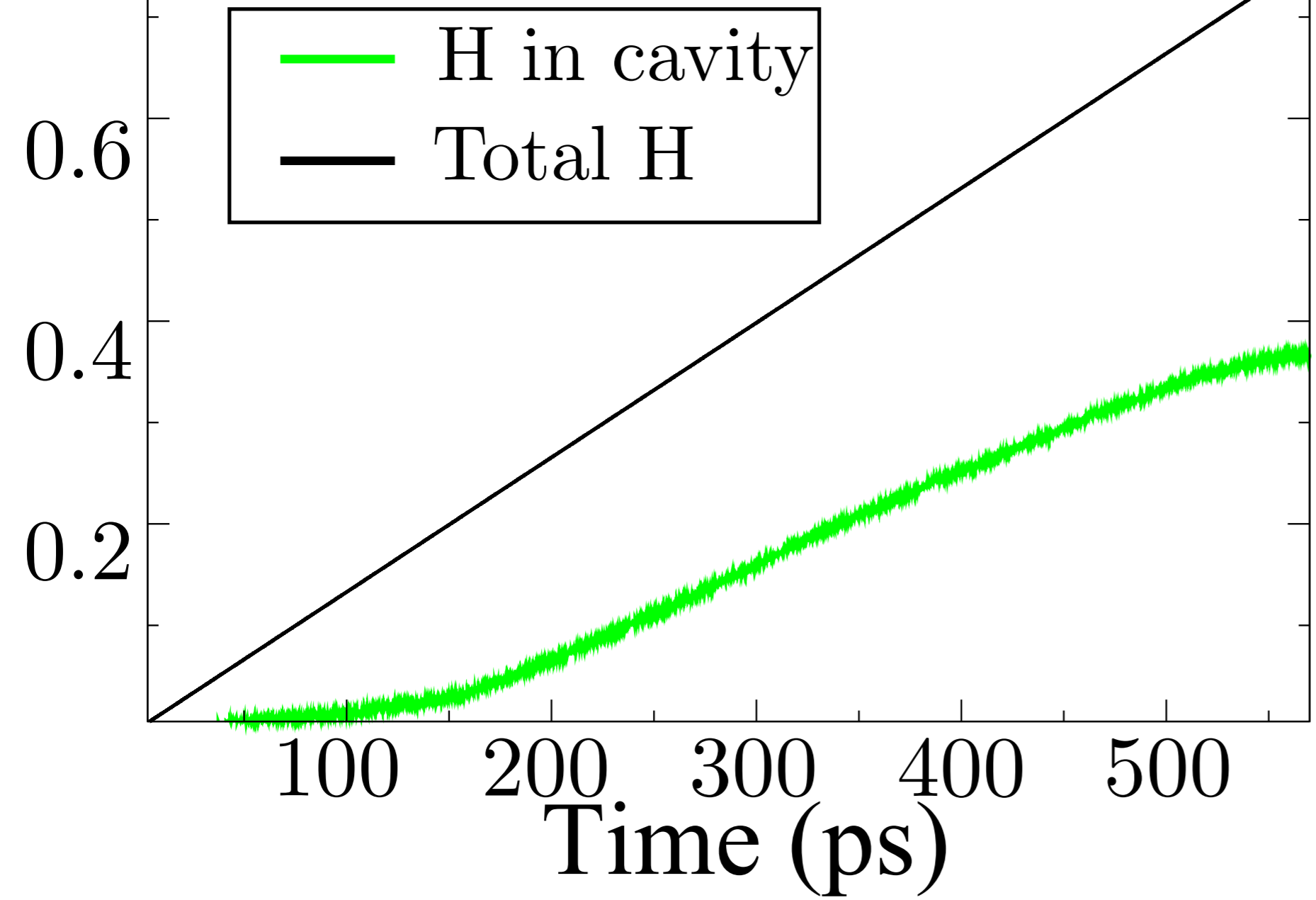
- 1
2
3
4 (31) Daw, M. S.; Baskes, M. I. Embedded-Atom Method: Derivation and Application to
5 Impurities, Surfaces, and other Defects in Metals. *Phys. Rev. B* **1984**, *29*, 6443.
6
7
8 (32) Zhou, X.; Zimmerman, J. A.; Wong, B. M.; Hoyt, J. J. An Embedded-Atom Method
9 Interatomic Potential for Pd–H Alloys. *J. of Materials Res.* **2008**, *23*, 704–718.
10
11
12 (33) Bitzek, E.; Koskinen, P.; Gähler, F.; Moseler, M.; Gumbsch, P. Structural Relaxation
13 Made Simple. *Phys. Rev. Lett.* **2006**, *97*, 170201.
14
15
16
17 (34) Van Duin, A. C.; Dasgupta, S.; Lorant, F.; Goddard, W. A. ReaxFF: a Reactive Force
18 Field for Hydrocarbons. *J. Phys. Chem. A* **2001**, *105*, 9396–9409.
19
20
21
22 (35) Senftle, T. P.; Janik, M. J.; van Duin, A. C. A ReaxFF Investigation of Hydride Forma-
23 tion in Palladium Nanoclusters via Monte Carlo and Molecular Dynamics Simulations.
24
25
26
27
28
29
30 (36) Langhammer, C.; Zhdanov, V. P.; Zorić, I.; Kasemo, B. Size-Dependent Kinetics of
31 Hydriding and Dehydriding of Pd Nanoparticles. *Phys. Rev. Lett.* **2010**, *104*, 135502.
32
33
34 (37) Hara, S.; Caravella, A.; Ishitsuka, M.; Suda, H.; Mukaida, M.; Haraya, K.; Shimano, E.;
35
36
37
38
39
40
41
42
43
44
45
46
47
48
49
50
51
52
53
54
55
56
57
58
59
60 (38) Pauling, L. *The Nature of the Chemical Bond and the Structure of Molecules and Crystals: an Introduction to Modern Structural Chemistry*; Cornell University Press, 1960; Vol. 18.

(39) Du, Q.; Faber, V.; Gunzburger, M. Centroidal Voronoi Tessellations: Applications and Algorithms. *SIAM Review* **1999**, *41*, 637–676.

(40) Honeycutt, J. D.; Andersen, H. C. Molecular Dynamics Study of Melting and Freezing of Small Lennard-Jones Clusters. *J. of Phys. Chem. C* **1987**, *91*, 4950–4963.

- 1
2
3
4
5
6
7
8
9
10
11
12
13
14
15
16
17
18
19
20
21
22
23
24
25
26
27
28
29
30
31
32
33
34
35
36
37
38
39
40
41
42
43
44
45
46
47
48
49
50
51
52
53
54
55
56
57
58
59
60
- (41) Stukowski, A. Visualization and Analysis of Atomistic Simulation Data with OVITOthe Open Visualization Tool. *Modelling and Simulation in Materials Sci. and Eng.* **2010**, *18*, 015012.
- (42) Stukowski, A. Structure Identification Methods for Atomistic Simulations of Crystalline Materials. *Modelling and Simulation in Materials Science and Engineering* **2012**, *20*, 045021.
- (43) Jiang, L.; Yin, X.; Zhao, J.; Liu, H.; Liu, Y.; Wang, F.; Zhu, J.; Boey, F.; Zhang, H. Theoretical Investigation on the Thermal Stability of Hollow Gold Nanoparticles. *J. of Phys. Chem. C* **2009**, *113*, 20193–20197.
- (44) Huang, R.; Shao, G.-F.; Zeng, X.-M.; Wen, Y.-H. Diverse Melting Modes and Structural Collapse of Hollow Bimetallic Core-Shell Nanoparticles: A Perspective from Molecular Dynamics Simulations. *Sci. Rep.* **2014**, *4*, 2045.
- (45) Jiang, S.; Zhang, Y.; Gan, Y.; Chen, Z.; Peng, H. Molecular Dynamics Study of Neck Growth in Laser Sintering of Hollow Silver Nanoparticles with Different Heating Rates. *J. of Physics D: Appl. Phys.* **2013**, *46*, 335302.
- (46) Idrissi, H.; Wang, B.; Colla, M. S.; Raskin, J. P.; Schryvers, D.; Pardoën, T. Ultrahigh Strain Hardening in Thin Palladium Films with Nanoscale Twins. *Advanced Materials* **2011**, *23*, 2119–2122.

1
2
3
4
5
6
7
8
9
10
11
12
13
14
15
16
17
18
19
20
21
22
23
24
25
26
27
28
29
30
31
32
33
34
35
36
37
38
39
40
41
42
43
44
45
46
47
48
49
50
51
52
53
54
55
56
57
58
59
60



Structure analysis of hNP
for H/Pd=0.89

